Available online at www.sciencedirect.com
ScienceDirect
Journal of the European Ceramic Society 30 (2010) 1679–1690
www.elsevier.com/locate/jeurceramsoc

Phase-transformation and grain-growth kinetics in yttria-stabilized tetragonal zirconia polycrystal doped with a small amount of alumina

Koji Matsui [a,*], Hidehiro Yoshida [b], Yuichi Ikuhara [c]

[a] *Tokyo Research Laboratory, Tosoh Corporation, 2743-1, Hayakawa, Ayase, Kanagawa 252-1123, Japan*
[b] *National Institute for Materials Science, 1-2-1 Sengen, Tsukuba, Ibaraki 305-0047, Japan*
[c] *Institute of Engineering Innovation, School of Engineering, The University of Tokyo, 2-11-16, Yayoi, Bunkyo-ku, Tokyo 113-8656, Japan*

Received 31 July 2009; received in revised form 15 December 2009; accepted 6 January 2010
Available online 1 February 2010

Abstract

Microstructure development during sintering in 3 mol% Y_2O_3-stabilized tetragonal zirconia polycrystal doped with a small amount of Al_2O_3 was investigated in the isothermal sintering conditions of 1300–1500 °C. At the low sintering temperature at 1300 °C, although the density was relatively high, the grain-growth rate was much slow. In the specimen sintered at 1300 °C for 50 h, Y^{3+} and Al^{3+} ions segregated along grain boundaries within the widths of about 10 and 6 nm, respectively. In grain interiors, the cubic-phase regions were formed by not only a grain-boundary segregation-induced phase-transformation mechanism but also by spinodal decomposition. The grain-growth behavior was kinetically analyzed using the grain-size data in 1300–1500 °C, which indicated that the grain-growth rate was enhanced by Al_2O_3-doping. These phase-transformation and grain-growth behaviors are reasonably explained by the diffusion-enhanced effect of Al_2O_3-doping.

Keywords: Grain-boundary segregation-induced phase-transformation; Grain growth; Diffusion; ZrO_2; Al_2O_3

1. Introduction

Y_2O_3-stabilized tetragonal ZrO_2 polycrystal (Y-TZP) doped with a small amount of Al_2O_3 is excellent not only in mechanical properties, such as high fracture strength, toughness, and hardness but also in the resistance performance of low-temperature degradation that is given as an indication of reliability because the starting raw powder can be sintered at a low temperature.[1] These properties strongly depend on the microstructure in Y-TZP doped with a small amount of Al_2O_3, which is controlled by the sintering condition. Therefore, clarification of the microstructure-development mechanism during sintering in Y-TZP doped with a small amount of Al_2O_3 is important to further improve the properties in Y-TZP ceramics.

So far, the densification behavior and microstructure development during sintering in Y-TZP doped with Al_2O_3 have been investigated by several researchers.[2–11] Matsui et al. have kinetically analyzed the densification behavior at the initial sintering stage in 3 mol% Y-TZP powder compacts with 0–1 mass% Al_2O_3.[2] According to their results, the densification rate increased with increasing Al_2O_3 concentration, which is explained by the increase in apparent frequency-factor term in the rate constant. Sakka et al.[3] have reported that the grain growth in 3 mol% Y-TZP is controlled by cation diffusion, which is enhanced by adding Al_2O_3. Guo and Waser have investigated the effects of Al_2O_3 on grain-boundary electrical properties in Y-TZP.[4] In previous papers, we have analyzed the microstructure in 3 mol% Y-TZPs doped with 0.3 mol% Al_2O_3 sintered at various temperatures for 2 h, and reported that the tetragonal-to-cubic ($T \rightarrow C$) phase-transformation mechanism is reasonably explained using a *grain-boundary segregation-induced phase-transformation* (*GBSIPT*) model.[5,6] Furthermore, our results showed that Al^{3+} ions segregated at grain boundaries directly relate to acceleration of the densification rate and these segregated Al^{3+} ions clearly enhance $T \rightarrow C$ phase transformation and grain growth at sintering temperatures above 1500 °C.[6]

It is important to examine the $T \rightarrow C$ phase-transformation behavior at a low sintering temperature to understand the

* Corresponding author at: Tosoh Corporation, Tokyo Research Laboratory, 2743-1, Hayakawa, Ayase, Kanagawa 252-1123, Japan. Tel.: +81 467 77 3851; fax: +81 467 77 3856.
E-mail address: kouji-matsui-nb@tosoh.co.jp (K. Matsui).

0955-2219/$ – see front matter © 2010 Elsevier Ltd. All rights reserved.
doi:10.1016/j.jeurceramsoc.2010.01.007

relationships between microstructure and properties (i.e., mechanical and degradation-resistance performances) in Y-TZP doped with a small amount of Al_2O_3 because the starting raw powder can be sintered at the low sintering temperature by the densification-acceleration effect of Al_2O_3-doping. However, the $T \rightarrow C$ phase-transformation behavior at such a low temperature has not been reported previously. On the other hand, the isothermal sintering measurement has an advantageous as an experimental method that can separate $T \rightarrow C$ phase-transformation and grain-growth behaviors, and the $T \rightarrow C$ phase-transformation behavior without grain growth can be examined by selecting the low sintering temperature.[12] Furthermore, the grain-growth mechanism can be discussed by kinetically analyzing the grain-size change during isothermal sintering. Therefore, the microstructural analysis at isothermal sintering is needed to quantitatively understand the $T \rightarrow C$ phase-transformation mechanism at the low sintering temperature and the grain-growth mechanism during sintering in Y-TZP doped with a small amount of Al_2O_3.

In the present study, we investigated microstructure development under the isothermal conditions of 1300–1500 °C for 0–50 h in order to verify the $T \rightarrow C$ phase-transformation behavior at the low sintering temperature and clarify the grain-growth mechanism in 3 mol% Y-TZP doped with 0.3 mol% Al_2O_3. The $T \rightarrow C$ phase-transformation behavior at the low sintering temperature was analyzed at 1300 °C. The grain-growth behavior was kinetically analyzed using the grain-size data in 1300–1500 °C. The $T \rightarrow C$ phase-transformation behavior at 1300 °C and the grain-growth mechanism in 3 mol% Y-TZP doped with 0.3 mol% Al_2O_3 were discussed based on the present results.

2. Experimental procedure

2.1. Specimen preparation

3 mol% (5.2 mass%) Y-TZP powder with 0.3 mol% (0.25 mass%) Al_2O_3 and a 15 m^2/g specific surface area (TZ-3Y-E grade, Tosoh, Tokyo, Japan), manufactured by the hydrolysis process, was used as a starting raw material. This powder was pressed uniaxially into a disk under 70 MPa pressure. Isothermal sintering was conducted for the powder compacts as follows: the temperature of the specimens in air was raised at a constant rate of 100 °C/h to the set temperature that was the range of 1300–1500 °C, and held in the range of 0–50 h. The specimens of the resulting Y-TZPs doped with Al_2O_3 are termed 3YE.

In previous papers, we did not report the analytical result for grain-boundary energy in 3 mol% Y-TZP (without Al_2O_3-doping).[12–14] Therefore, 3 mol% Y-TZP specimens for grain-boundary energy measurement were prepared by the same pressing and sintering conditions as those described above, using the 3 mol% (5.2 mass%) Y-TZP powder without Al_2O_3 and a 15 m^2/g specific surface area (TZ-3Y grade, Tosoh, Tokyo, Japan). The specimens are termed 3Y.

2.2. Density and grain-size measurements

The density of sintered specimens was measured by the Archimedes method. Scanning electron microscopy (SEM; Model S-4500, Hitachi, Tokyo, Japan) was used to measure the average grain sizes of the sintered specimens. SEM specimens were polished with a diamond paste of 3 μm and then thermally etched for 1 h at a temperature that was 50 °C lower than the sintering temperature of each specimen in air. The average grain size was measured by the Planimetric method.[15]

2.3. XRD measurements

X-ray diffraction (XRD) profiles were measured in the diffraction-angle (2θ) range of 20–90° and at room temperature using a powder diffractometer system (Model MXP^3, MAC Science Co. Ltd., Tokyo, Japan) and recorded using Cu$K\alpha$ radiation, under 40 kV and 30 mA, at a slit width of 1°. Using RIETAN94[16] as the analytical program, the mass fraction of cubic phase (f_c) in the sintered bodies was determined by the Rietveld method.[17] According to the Rietveld analysis, the mass fraction of each phase in a mixture of multiphase can be estimated from the scale factors determined precisely.[18] The analysis was dealt with as the dual-phase mixture which comprised of tetragonal and cubic phases because the reflections assigned to the monoclinic phase were not observed. The Rietveld calculation was conducted in the same manner reported by Ohmichi et al.[19]

2.4. Estimation of grain-boundary energy

The grain-boundary energy of sintered specimens was estimated by a conventional thermal grooving technique.[20,21] The grain-boundary energy (γ_{gb}) is given by the following equation[22]:

$$\gamma_{gb} = 2\gamma_s \cos\left(\frac{\phi}{2}\right) \quad (1)$$

where γ_s is the surface energy and ϕ is the dihedral angle on the thermally grooved grain boundary. The ϕs were directly measured from the groove profiles obtained by atomic force microscopy (AFM; SPM-9500J2, Shimadzu Co., Kyoto, Japan). AFM specimens were polished and then thermally etched in the same condition as SEM-specimen preparation described above. The ϕ was measured at 120 different points for each grain boundary. The γ_{gb} cannot directly determined using Eq. (1) because both values of γ_s in 3 mol% Y-TZPs doped with and without Al_2O_3 have not been reported previously. Therefore, the γ_{ngb} was estimated as the normalized grain-boundary energy that is defined by Kuwabara et al.[20] Using Eq. (1), the γ_{ngb} is defined by the following equation:

$$\gamma_{ngb} \equiv \frac{\gamma_{gb}}{\gamma_s} = 2\cos\left(\frac{\phi}{2}\right) \quad (2)$$

2.5. TEM and nanoprobe EDS measurements

The microstructures were examined using a field emission transmission electron microscope (TEM; Model 002BF, Topcon, Tokyo, Japan). Specimens for TEM observations were mechanically ground to a thickness of ~0.1 mm, further dimpled to a thickness of ~10 μm, and then ion-milled for electron transparency. High-resolution transmission electron microscopy (HRTEM) observations were conducted to examine the grain-boundary structures, using the TEM with a point-to-point resolution of 0.17 nm. Nanoprobe X-ray energy-dispersive spectroscopy (EDS) measurements were performed to quantitatively examine the segregation of Y^{3+} and Al^{3+} ions at grain boundaries, using a Noran Voyager System in the TEM with a probe size of about 0.5 nm. Four to five edge-on grain boundaries were analyzed in one specimen. STEM-nanoprobe EDS element mappings were also performed to examine the Y^{3+} and Al^{3+} ion distributions within grains, using the Noran Voyager System in the TEM.

3. Results and discussion

3.1. Densification and grain-growth behaviors at 1300–1500 °C

Fig. 1(a) shows the plots of relative density in 3YEs as a function of holding time at sintering temperatures of 1300–1500 °C. In the 3YE sintered at 1300 °C for 0 h, the relative density attained 91.5%. The relative density increased with increasing holding time, and attained 99.4% at 1300 °C for 50 h. The densification rate enhanced with increasing sintering temperature. The grain-growth behavior at each sintering temperature was shown in Fig. 1(b). Here, each curve of grain-growth behavior is that calculated using the rate equation of grain growth that is derived in Section 3.4. At 1300 °C, the grain growth was very limited, while the grain size significantly increased at the sintering temperature more than 1400 °C. As an instance, SEM images in 3YEs sintered at (a) 1300°C and (b) 1500 °C for 50 h were shown in Fig. 2.

3.2. Microstructure development at 1300 °C

3.2.1. Formation behavior of the cubic phase

Fig. 3(a) shows XRD profiles in 3YEs sintered at 1300 °C for 2 and 50 h. The profiles were enlarged in the 2θ range of 72–76° because the range can visually distinguish reflection peaks of tetragonal from cubic phases (Fig. 3(b)). In the 3YE sintered for 2 h, $(0\,0\,4)_t$ and $(2\,2\,0)_t$ reflection peaks that are assigned to the tetragonal phase were observed. In the 3YE sintered for 50 h, however, the $(4\,0\,0)_c$ reflection peak that is assigned to the cubic phase clearly appeared. This result indicates that the cubic phase forms during isothermal sintering even at 1300 °C. Therefore, using the XRD profiles measured in the 2θ range of 20–90°, the Rietveld calculation was conducted to quantitatively determine the formed amount of the cubic phase. The reliability factors (R_{wp}) obtained were in the range of 6.5–7.2, which correspond nearly to the analytical results (R_{wp} = 5.3–6.8) in 3 mol% Y-TZP reported by Ohmichi et al.[19] Fig. 4 shows the plot of f_c against holding time in 3YE sintered at 1300 °C. The cubic phase was observed at 0 h and the f_c was estimated to be 11 mass%. The f_c increased with increasing holding time, and attained 15 mass% at 50 h. This behavior is interpreted by the increase in cubic phase formed by the $T \rightarrow C$ phase transformation.

3.2.2. Grain-boundary segregation

Fig. 5 shows the typical conventional bright-filed TEM image in 3YE sintered at 1300 °C for 50 h. The grain-boundary faces were straight and their grain corners were angular. Fig. 6 shows the typical HRTEM image of the grain boundary in 3YE sintered at 1300 °C for 50 h. The HRTEM image was taken with

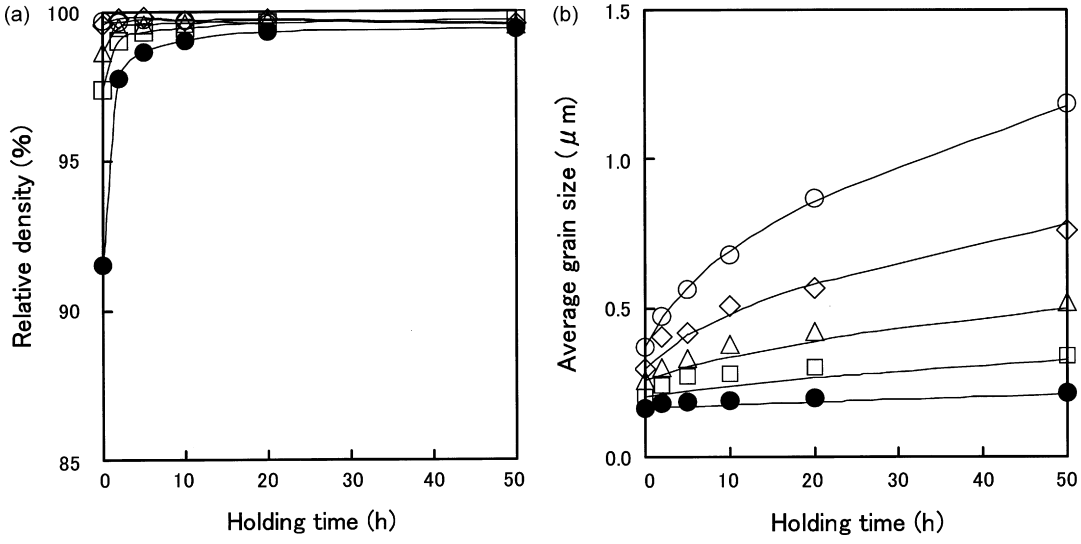

Fig. 1. Plots of (a) relative density and (b) average grain size in 3YEs as a function of holding time at sintering temperatures of 1300–1500 °C: (●) 1300 °C, (□) 1350 °C, (△) 1400 °C, (◇) 1450 °C, and (○) 1500 °C. Solid lines in (b) indicate the calculated curves.

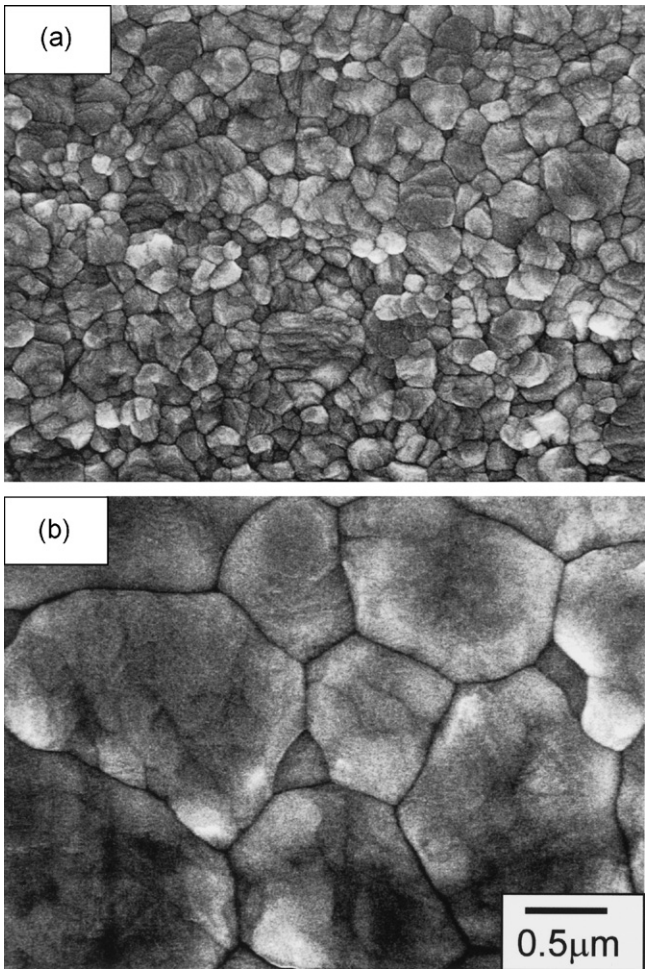

Fig. 2. SEM images in 3YEs sintered at (a) 1300°C and (b) 1500 °C for 50 h.

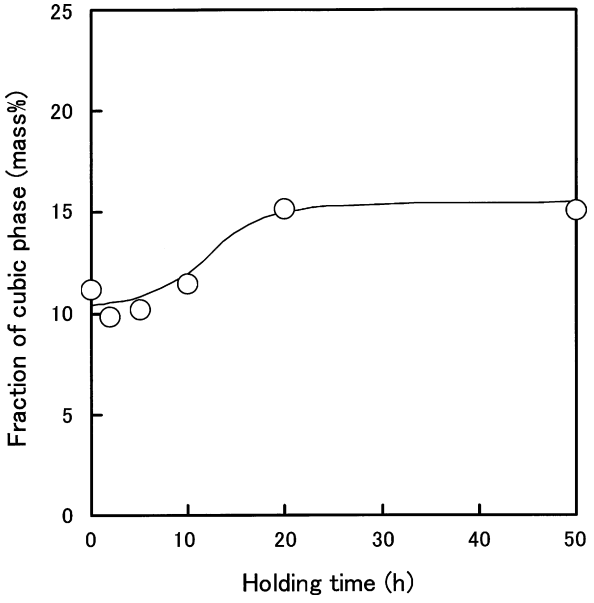

Fig. 4. Plots of cubic-phase fraction in 3YEs as a function of holding time at 1300 °C.

the boundary at the edge-on condition to directly observe the grain-boundary structure. In the HRTEM image, no amorphous or second phase was observed along the grain-boundary faces. Electron-diffraction patterns showed that the both grains were assigned to the tetragonal phase. This observation agrees with previous data in 3YE sintered at 1300 °C for 2 h.[5,6]

Fig. 7(a) and (b) shows two types of typical Y-concentration profile across the grain boundary in 3YE sintered at 1300 °C for 50 h. In Fig. 7(a), the Y_2O_3 concentrations in grain interior were in a range of 1.8–2.2 mol%, which is consistent with that in the tetragonal phase. The Y_2O_3 concentration is significantly high in the vicinity of the grain boundary, and the Y-concentration is

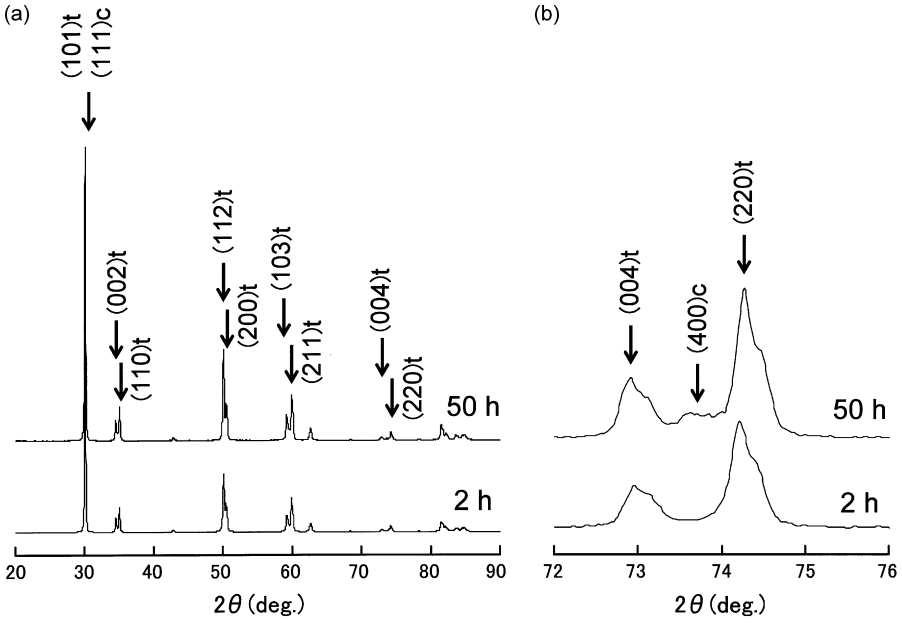

Fig. 3. XRD profiles in 3YEs sintered at 1300 °C for 2 and 50 h: (a) all measured regions and (b) enlargement of the 2θ range of 72–76°.

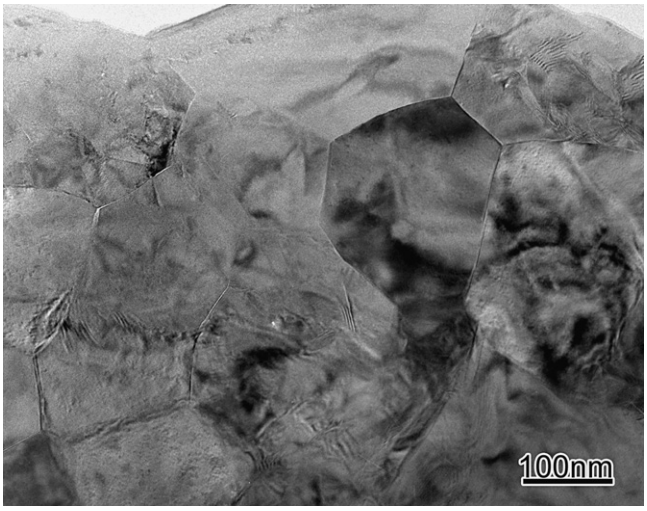

Fig. 5. Conventional bright-field TEM image in 3YE sintered at 1300 °C for 50 h.

4.3 mol% just on the grain boundary. This fact indicates that Y^{3+} ions segregated at the grain boundaries over a width below about 10 nm in all grain boundaries between tetragonal and tetragonal phases (*T–T* grain boundaries). This result is consistent with the *T–T* grain boundary shown in Fig. 6. The different Y-concentration profile (Fig. 7(b)) was also observed in the present specimen; in Fig. 7(b), the Y-concentration in the left side is around 1.9 mol%, but steeply increases near the grain boundary. The Y-concentration in the right side is about 7.3 mol%, which is close to that of cubic rather than tetragonal phases. In previous papers, we reported that no grain with a high Y-concentration was observed in the 3YE sintered at 1300 °C for 2 h.[5,6] Taking into account our previous result, this grain of the high Y-concentration is the cubic grain formed during the holding time of 50 h. Therefore, this phase interface is concluded to the grain boundary between cubic and tetragonal phases (*C–T* grain boundary).

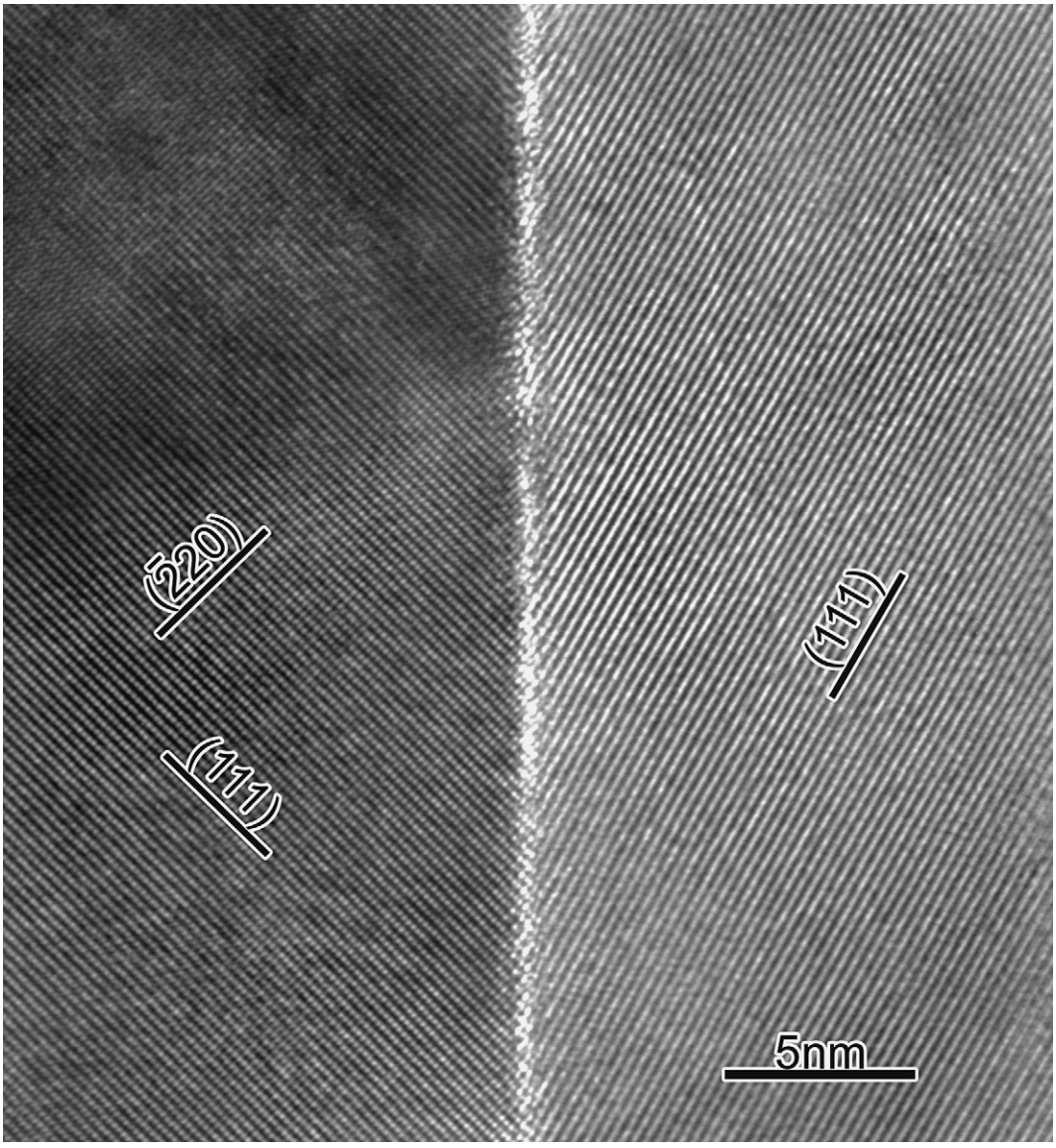

Fig. 6. HRTEM image of the grain boundary in 3YE sintered at 1300 °C for 50 h.

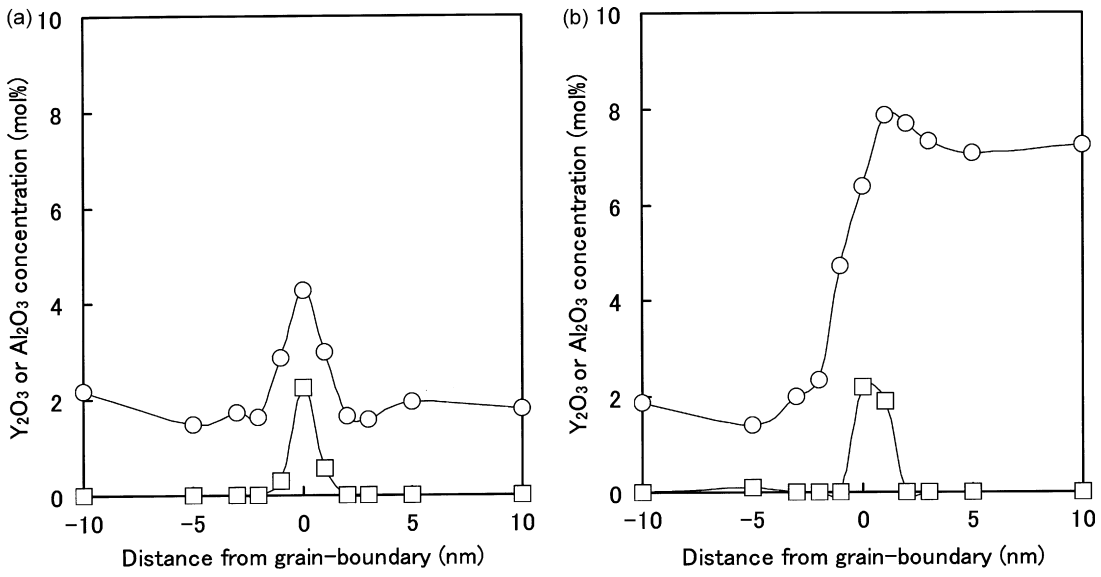

Fig. 7. Y- and Al-concentration profiles across the grain boundaries in 3YEs at 1300 °C for 50 h: (a) *T–T* and (b) *C–T* grain boundaries.

Al-concentration profiles across grain boundaries were also plotted in Fig. 7(a) and (b). Al^{3+} ions segregate at both *T–T* and *C–T* grain boundaries over a width of about 6 nm. This result also agreed with previous data in 3YE sintered at 1300 °C for 2 h.[5,6]

3.2.3. Grain-interior microstructure

Fig. 8 shows (a) STEM, (b) Zr-*Kα* mapping, (c) Y-*Kα* mapping, and (d) Al-*Kα* mapping images in 3YE sintered at 1300 °C for 50 h. The Y-*Kα* mapping image (Fig. 8(c)) clearly shows the grain-boundary segregation of Y^{3+} ions, which is consistent

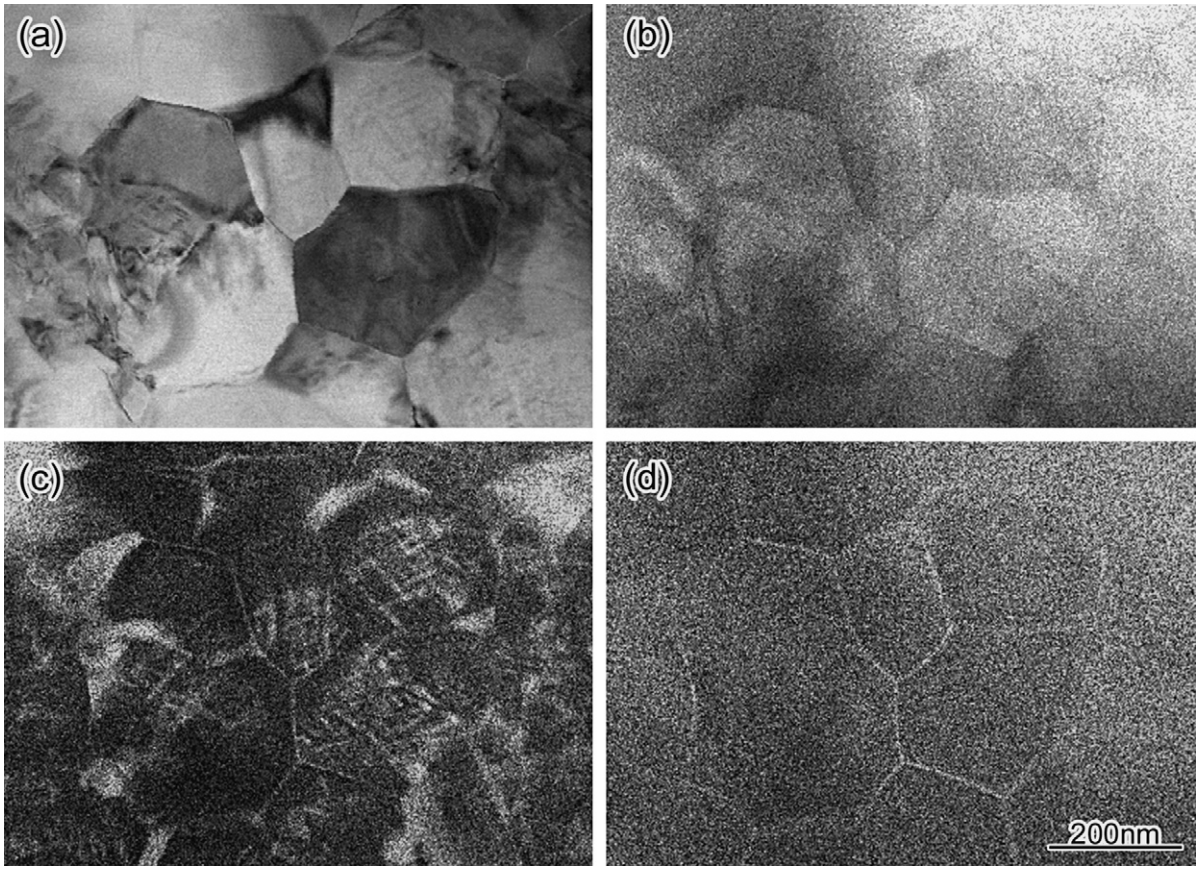

Fig. 8. STEM image, and Zr-*Kα*, Y-*Kα*, and Al-*Kα* mapping images by STEM-nanoprobe EDS method, in 3YE sintered at 1300 °C for 50 h: (a) STEM image, (b) Zr-*Kα* mapping image, (c) Y-*Kα* mapping image, and (d) Al-*Kα* mapping image. Bright parts in the Y-*Kα* and Al-*Kα* mapping images correspond to regions with high Y^{3+} and Al^{3+} ion concentrations, respectively.

with that in Fig. 7(a). In the grain interiors, the regions with high Y^{3+} ion concentrations were formed adjacent to the grain boundary, which seem to be started to form from the grain boundaries and/or triple junctions. Furthermore, the modulated pattern with high Y^{3+} ion concentration was observed inside grains, which is likely to be the modulated structure formed by spinodal decomposition.[23–26] According to the report in Sakuma et al.,[24] spinodal decomposition occurs in 2.5–6 mol% Y_2O_3-stabilized ZrO_2 under the isothermal annealing condition of 1300 °C. Shibata et al.[26] have showed that the modulated structure formed by spinodal decomposition in 6 mol% Y_2O_3-stabilized ZrO_2 is the lamellate constituted from two *T–C* regions and the about 15 nm wavelength. The present result is also observed in the similar modulated structure at the isothermal sintering process. Therefore, the modulated structure in Y-*Kα* mapping image is formed by spinodal decomposition accompanied by $T \rightarrow C$ phase transformation.

In previous papers, we reported the microstructure in 3YE sintered at 1300 °C for 2 h, as described below.[5,6] The distribution of Y^{3+} ions in grain interiors was almost homogeneous, which indicated that the interiors of most grains were the tetragonal phase. On the other hand, most of the grain boundaries where Y^{3+} ions segregate transformed from tetragonal-to-cubic phases.[6] As shown in Fig. 4, in the isothermal sintering process at 1300 °C, the f_c increased with increasing holding time. Therefore, both high Y^{3+} ion concentration regions that are adjacent to grain boundaries and that are formed by spinodal decomposition in the grain interiors should be the cubic phase that was formed by $T \rightarrow C$ phase transformation. According to the result in Fig. 7(b), it is reasonable that the cubic-phase region that is adjacent to the grain boundaries was formed from grain boundaries.

The Al-*Kα* mapping measurement was also performed because a small amount of Al_2O_3 was doped to 3YE. As shown in the Al-*Kα* map (d), Al^{3+} ions were also observed to segregate along grain boundaries. This result is consistent with that in Fig. 7. The phase diagram of the ZrO_2–Al_2O_3 system has been reported previously,[27] though that of the ZrO_2–Y_2O_3–Al_2O_3 system is not known. According to the phase diagram reported, ZrO_2 and Al_2O_3 exhibit very limited mutual solubility, and the solubility of Al_2O_3 in ZrO_2 increases with increasing temperature. Hodgson *et al*. have estimated that the solubility of Al_2O_3 is about 0.1% at 1300 °C.[8] Therefore, taking into account the results in Figs. 7 and 8(d), a small amount of Al_2O_3 doped in 3YE is almost present in the grain-boundary vicinities and slightly present in the grain interiors during isothermal sintering.

3.3. $T \rightarrow C$ phase-transformation and grain-growth behaviors at 1300 °C

In previous papers, we proposed the *GBSIPT* model as the $T \rightarrow C$ phase-transformation mechanism in Y-TZP, as described below.[12–14] According to the phase diagram for the ZrO_2–Y_2O_3 system, the crystal phases in Y-TZP exit as the tetragonal–cubic (*T–C*) dual-phase at equilibrium temperatures above about 600 °C, and the mole fraction of cubic phase increases with increasing equilibrium temperature.[28] The segregation of Y^{3+} ions in Y-TZP is caused by the driving force for *T–C* dual-phase partitioning. The amount of segregated Y^{3+} ions increases with increasing sintering temperature. When the sintering temperature at which the cubic phase is thermodynamically stable is attained, the cubic phase starts to form from grain boundaries and/or triple junctions in which Y^{3+} ions segregate because the segregation regions of Y^{3+} ions have a strong tendency to cause $T \rightarrow C$ phase transformation. Further, when the sintering temperature increases, the cubic-phase regions are formed in grain interiors adjacent to the grain boundaries with grain growth. Therefore, the diffusion of Y^{3+} ions for forming the cubic-phase regions is also caused by the driving force for *T–C* dual-phase partitioning. The $T \rightarrow C$ phase-transformation behavior in 3YEs sintered at various temperatures for 2 h is also explained by the *GBSIPT* model.[5,6]

On the other hand, the $T \rightarrow C$ phase-transformation behavior in 3YE during isothermal sintering at 1300 °C is discussed as follows. In the 3YE sintered at 1300 °C for 2 h, the Y^{3+} ion distribution in grain interiors was nearly homogeneous, but Y^{3+} and Al^{3+} ions segregated at grain boundaries over the widths below about 10 and 6 nm, respectively,[5,6] and the vicinity of the grain boundaries transforms from tetragonal-to-cubic phases.[6] When the holding time increases from 2 to 50 h at the constant temperature of 1300 °C, the grain growth is very limited (negligible), but Y^{3+} ions in the grain-interior region near to the grain-boundary vicinity diffuse to grain boundaries and/or triple junctions to form the cubic-phase region, and then cubic-phase regions are formed in grain interiors adjacent to the grain boundaries (i.e., the *GBSIPT* mechanism). Ii et al. have analyzed the interphase boundary between cubic and tetragonal phases co-existed into a single grain formed during sintering in 3 mol% Y-TZP.[29] They showed that misfit dislocations caused by the difference in tetragonal- and cubic-lattice parameters are present at the interphase boundary, and the Y^{3+} ion concentration changes sharply at the interphase boundary with a transition width of about 10 nm. This indicates that misfit dislocations are generated at the interphase boundary between cubic-phase and tetragonal-phase regions in grain interiors formed by the *GBSIPT* mechanism.

Furthermore, in this isothermal sintering condition, the modulated structure of the cubic phase is also generated in the grain-interior region away from the grain-boundary vicinity by spinodal decomposition. Spinodal decomposition in the *T–C* dual-phase region are thermodynamically understand by a concept of the free energy–composition diagram (*G–x* diagram) proposed by Sakuma et al.[24] According to their concept, in the *T–C* dual-phase region at a certain temperature, tetragonal and cubic phases are given as the single continuous *G–x* curve, and spinodal decomposition occurs in the composition range between two inflection points (i.e., $\partial G^2/\partial x^2 = 0$) in the *G–x* curve. The composition range at 1300 °C is estimated to that of 2.5–6 mol% Y_2O_3 inside the *T–C* dual-phase region.[24] Therefore, spinodal decomposition in 3YE spontaneously progresses during isothermal sintering at 1300 °C because the composition is 3 mol% Y_2O_3, and the modulated structure is formed by the up-hill diffusion of Y^{3+} ions that is caused by the driving force

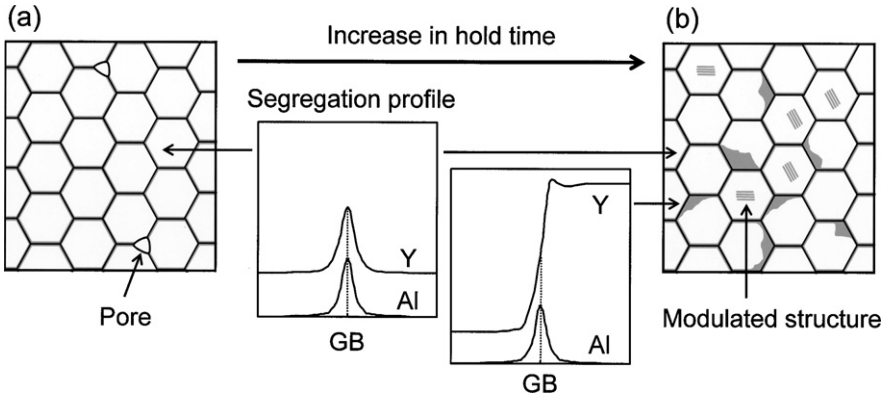

Fig. 9. Scheme of the *T–C* phase-transformation mechanism in 3YE during isothermal sintering at 1300 °C: (a) 2 h and (b) 50 h. The gray parts of the grain boundary indicate segregation of Y^{3+} and Al^{3+} ions. The white and gray regions of grain interior represent the tetragonal and cubic phases, respectively. GB is grain boundary.

for *T–C* dual-phase partitioning. The movement of the grain boundary in which Y^{3+} ions segregate disintegrates the modulated structure that is generated in the grain interior. Therefore, in the 3YE sintered at 1300 °C for 50 h, the modulated structure of the cubic phase is considered to be formed in grain interiors because of the very limited grain growth.

On the contrary, the modulated structure was not clearly observed in 3 mol% Y-TZP (without Al_2O_3-doping) sintered at 1300 °C for 50 h.[12] In isothermal sintering at 1300 °C, although the grain-growth behavior in 3 mol% Y-TZP is almost the same as that in 3YE, the densification rate in 3 mol% Y-TZP is much slower than that in 3YE.[12] Sakka et al. have reported that the cation diffusion in the Y_2O_3– and CeO_2–$(Zr_{1-x}Hf_x)O_2$ systems is much smaller than the oxygen diffusion.[30,31] Therefore, the densification rate in 3 mol% Y-TZP is controlled by the cation diffusion of Zr^{4+} and Y^{3+} ions, which is remarkably enhanced by Al_2O_3-doping. This Al_2O_3-doping effect is discussed as follows. According to the sintering kinetic analysis reported by Matsui et al., the densification rate at the initial sintering stage in 3 mol% Y-TZP is remarkably accelerated by Al_2O_3-doping, and the accelerated effect is explained by the increase in apparent frequency-factor term in the sintering-rate constant.[2] They discussed that the increase in apparent frequency-factor term is related to oxygen vacancies generated by the Al_2O_3-dpoing reaction. Yoshida et al.[32] have reported the effect of a small amount of dopant (BaO, MgO, TiO_2, and GeO_2) on microstructure development in 3 mol% Y-TZP. They experimentally showed that the grain-boundary diffusivity at 1400 °C increased with decreasing ionic radius of dopant, and discussed that the behavior is related to the atomic interaction between the grain boundary and the segregated dopant cations. Furthermore, the factor of electrostatic charge compensation[33] also influences the atomic interaction, which is related to the charge difference between Zr^{4+} ions and dopant cations. The ionic radius of Al^{3+} ions (0.068 nm) is smaller than those of Zr^{4+} (0.086 nm) and Y^{3+} ions (0.104 nm)[34]; the charge of Al^{3+} ions is different from that of Zr^{4+} ions. As shown in Fig. 7, Al^{3+} ions segregate at grain boundaries in 3YE. It is therefore concluded that the cation diffusion is remarkably enhanced by the combined effect of oxygen vacancies formed by Al_2O_3-doping, and the ionic size and charge of Al^{3+} ions.

This Al_2O_3-doping accelerates the diffusion of Y^{3+} ions for causing *T–C* dual-phase partitioning, and Al_2O_3 which is solved in grain interiors by Al_2O_3-doping suggests that the up-hill diffusion of Y^{3+} ions tends to occur under the isothermal sintering condition of 1300 °C at which the grain growth is very limited. In 3 mol% Y-TZP, many interconnected and isolated pores remain in the isothermal sintering process at 1300 °C because the densification rate is much slower than that in 3YE.[12] At the densification stage with shrinkage and movement of such a pore, the modulated structure may be hard to be formed in grain interiors. Therefore, when the diffusion at the densification stage is enhanced by Al_2O_3-doping and the grain growth is very limited under the isothermal sintering condition at which the density is relatively high, the cubic-phase regions in grain interiors not only are formed adjacent to the grain boundaries by the *GBSIPT* mechanism but also are formed by spinodal decomposition. This $T \rightarrow C$ phase-transformation scheme in 3YE is shown in Fig. 9. The cubic-phase regions formed adjacent to the grain boundaries by the *GBSIPT* mechanism in 3YE (Fig. 8(c)) decrease as compared with the previous Y-*Kα* mapping data in 3 mol% Y-TZP sintered at 1300 °C for 50 h.[12] In the isothermal sintering condition of 1300 °C, the $T \rightarrow C$ phase transformation in 3YE may predominantly occurs by spinodal decomposition because of the Al_2O_3-doping effect.

In isothermal sintering at 1300 °C, the cation diffusion is enhanced by Al_2O_3-doping; nevertheless, the grain-growth behavior in 3YE is almost the same as that in 3 mol% Y-TZP.[12] The grain-growth behavior under this sintering profile is qualitatively discussed as follows. In the previous paper, we compared the microstructures in 3YE with 3 mol% Y-TZP sintered at 1100–1650 °C for 2 h.[6] According to this comparison, the increasing behavior of grain size in 3YE showed the same tendency as that in 3 mol% Y-TZP up to 1500 °C, but over this temperature, the grain size in 3YE became larger than that in 3 mol% Y-TZP. In the analytical result of grain-boundary segregation, the segregated amount of Y^{3+} ions in 3YE increased with increasing sintering temperature, which showed a tendency similar to the segregation behavior of Y^{3+} ions in 3 mol% Y-TZP. As with the segregation behavior of Y^{3+} ions, the segregated amount of Al^{3+} ions in 3YE increased with increasing sintering temperature. This indicates that although grain growth is controlled by

the segregated amount of Y^{3+} ions, when the segregated amount of Al^{3+} ions exceeds a certain value, grain growth is accelerated. Therefore, we concluded that the increase in grain size above 1500 °C in 3YE is caused by the effects of segregated Al^{3+} ions rather than segregated Y^{3+} ions. Taking into account this conclusion, the gain-growth behavior at 1300 °C in 3YE is controlled primarily by the effect of segregated Y^{3+} ions. This behavior is quantitatively discussed by kinetic analysis in Section 3.4.

3.4. Grain-growth mechanism

In the previous paper, we revealed that the grain-growth rate in Y-TZP is controlled by the concentration of Y^{3+} ions segregated at the grain boundary, whereas the cubic-phase regions in grain interiors do not effectively act the pinning points for retarding grain growth.[14] This grain-growth behavior can be quantitatively analyzed using the rate equation of the third-power growth low derived based on a solute-drag theory.[12] The rate equation (differential type) is given by

$$\frac{dD}{dt} = \frac{k_3}{D^2} \tag{3}$$

where D is the average grain size, t is the time, and k_3 is the growth constant which is usually expressed as[35]

$$k_3 = k_{03} \exp\left(-\frac{Q_3}{RT}\right) \tag{4}$$

Here, k_{03} is a pre-exponential term, Q_3 is the activation energy for causing grain growth, R is the gas constant, and T is the absolute temperature. In the solute-drag effect, the grain-boundary mobility depends on lattice diffusion (LD) of solute atoms segregated along the grain boundaries.[36] Therefore, the Q_3 is assigned to that for LD, i.e., diffusion through grain interior segregated with Y^{3+} ions.

On the other hand, Yoshida et al.[32] reported the effect of a small amount of dopant on the grain-growth behavior in Y-TZP. They experimentally showed that the dopant cations segregated along grain boundaries change grain-boundary diffusivity, which was discussed by the second-power growth low based on a single-phase material. This rate equation (differential type) is given by

$$\frac{dD}{dt} = \frac{k_2}{D} \tag{5}$$

where

$$k_2 = k_{02} \exp\left(-\frac{Q_2}{RT}\right) \tag{6}$$

Here, k_2 is the growth constant, k_{02} is a pre-exponential term, and Q_2 is the activation energy.[37] According to the discussion on the dopant effect in Yoshida et al.,[32] the Q_2 is assigned to that for grain-boundary diffusion (GBD), i.e., diffusion through grain boundary segregated with Al^{3+} ions.

In the present result, both Y^{3+} and Al^{3+} ions are observed to segregate along the grain boundaries because a small amount of Al_2O_3 is doped to 3YE (Fig. 7). It is therefore needed to derive the rate equation that is simultaneously applicable to LD for the solute-drag effect and GBD for the dopant effect in order to quantitatively analyze the grain-growth behavior in 3YE. In the previous paper, we discussed that segregated Al^{3+} ions in 3YE have the effect that enhances GBD, and at sintering temperatures above 1500 °C, the predominant effect that enhances grain growth is clearly caused by the effect of segregated Al^{3+} ions rather than the solute-drag effect of segregated Y^{3+} ions.[6] Analogizing from this result, it can be assumed that the grain-growth rate in 3YE is given as the sum of the right-hand sides of Eq. (3) (i.e., LD term that corresponds to the segregated Y^{3+} ion effect) and Eq. (5) (i.e., GBD term that corresponds to the segregated Al^{3+} ion effect), namely,

$$\frac{dD}{dt} = \frac{k_2}{D} + \frac{k_3}{D^2} \tag{7}$$

Integrating Eq. (7), one obtains

$$D^2 - 2\beta D + 2\beta^2 \ln(D+\beta) - \delta_0 = 2k_2 t \tag{8}$$

where

$$\beta = \frac{k_3}{k_2} \tag{9}$$

$$\delta_0 = D_0^2 - 2\beta D_0 + 2\beta^2 \ln(D_0+\beta) \tag{10}$$

Here, D_0 is the D at $t = 0$.

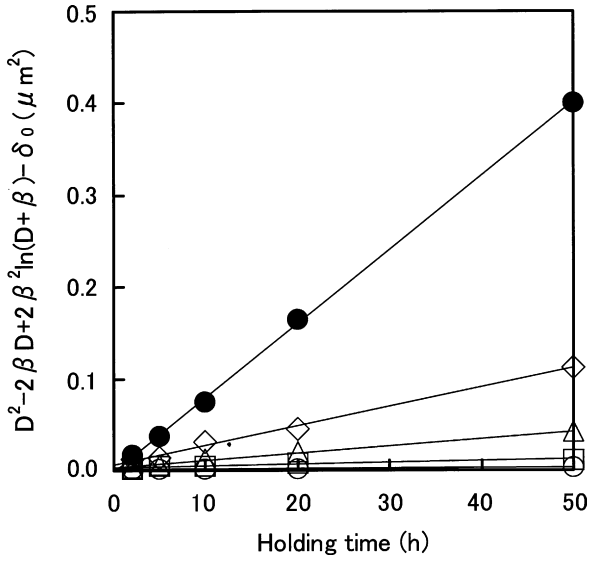

Fig. 10. Plots of $D^2 - 2\beta D + 2\beta^2 \ln(D+\beta) - \delta_0$ against holding time in 3YEs sintered at 1300 − 1500 °C: (◯)1300 °C, (□) 1350 °C, (△) 1400 °C, (◇) 1450 °C, and (●) 1500 °C. Each straight line was determined to fit the observed values.

Fig. 10 shows the plots of $D^2 - 2\beta D + 2\beta^2 \ln(D+\beta) - \delta_0$ against holding time in 3YE sintered at 1300–1500 °C. Here, the β at each sintering temperature was determined to fit the observed values: $\beta(1300\,^\circ\mathrm{C}) = 1.16$, $\beta(1350\,^\circ\mathrm{C}) = 1.49$, $\beta(1400\,^\circ\mathrm{C}) = 1.56$, $\beta(1450\,^\circ\mathrm{C}) = 1.87$, and $\beta(1500\,^\circ\mathrm{C}) = 1.80\,\mu\mathrm{m}$. The data for each sintering temperature showed a linear relationship because the correlation coefficient (r) was in the range of 0.938–1.00. The k_2 was determined from the slope of each straight line, and then the k_3 was obtained from Eq. (9). Fig. 11 shows the Arrhenius

Table 1
Activation energies and pre-exponential terms for causing grain growth in 3YE and 3 mol% Y-TZP.

Specimen	Activation energy (kJ/mol)		Pre-exponential term	
	Q_2	Q_3	$\ln[k_{02}, (m^2/s)]$	$\ln[k_{03}\ (m^3/s)]$
3YE	588	640	−1.48	−11.1
3 mol% Y-TZP[a]		618		−12.7

[a] The Q_3 and k_{03} in 3 mol% Y-TZP were determined using Eq. (3) and data in the previous paper[12].

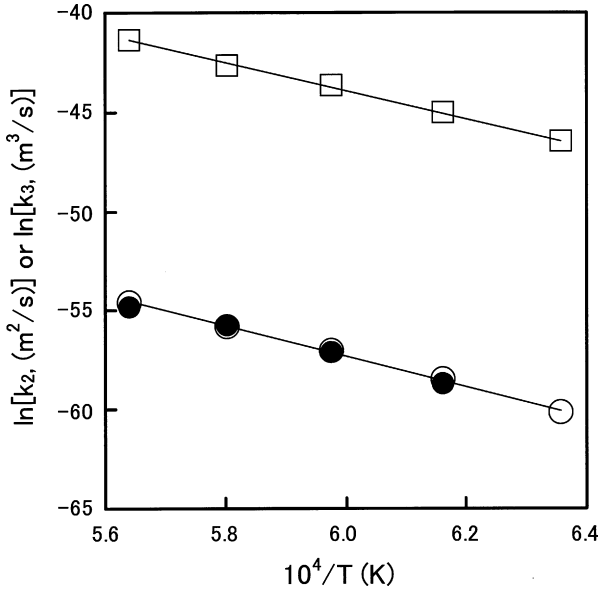

Fig. 11. Arrhenius plots of the growth constants in 3YE and 3 mol% Y-TZP. (□) and (◯) indicate k_2 and k_3 in 3YE, respectively. (●) indicates k_3 in 3 mol% Y-TZP.[11].

plot of natural logarithm k_2 or k_3 against $1/T$. These plots showed linear relationships (i.e., $r(k_2) = r(k_3) = -0.999$), and the Q_2, k_{02}, Q_3, and k_{03} were determined from the slopes and intercepts of the straight lines (Table 1). The Q_2 of the GBD term that corresponds to the segregated Al^{3+} ion effect was smaller than the Q_3 of the LD term that corresponds to the segregated Y^{3+} ion effect. To confirm the validity of the present analytical result, the time dependence of grain growth at each sintering temperature was calculated by substituting the values determined of Q_2, k_{02}, Q_3, and k_{03} in Eq. (8). As shown in Fig. 1(b), the time-dependent curves calculated fitted almost with the observed values, and this fitting result demonstrates that the Q_2, k_{02}, Q_3, and k_{03} determined are reasonable. Previous 3 mol% Y-TZP data were analyzed using the integral type of Eq. (3), i.e., $D^3 = D_0^3 + kt$ where the k is the growth constant.[12] Integrating Eq. (3), $D^3 = D_0^3 + 3k_3t$ is obtained. Therefore, each k in previous 3 mol% Y-TZP data[12] was converted to $k_3(=k/3)$, which was plotted in Fig. 11. The plot of natural logarithm k_3 against $1/T$ in 3 mol% Y-TZP exhibited a similar linear relationship to that in 3YE. In the previous paper, we concluded that although $\ln k_3$ at 1300 °C in 3 mol% Y-TZP was not estimated because most of the relative densities were in the range of intermediate sintering stage, the much slow grain-growth rate is caused by not only the retardation effect of residual pores but also the solute-drag effect of segregated Y^{3+} ions.[12] Estimating the $\ln k_3$ at 1300 °C by extrapolating the plots of 3 mol% Y-TZP in Fig. 11, $\ln k_3 = -60.0$ is obtained, which is approximately the same as the $\ln k_3(=-60.1)$ at 1300 °C in 3YE. This indicates that the k_2 (that corresponds to the segregated Al^{3+} ion effect) at 1300 °C in 3YE is negligibly small and the grain-growth rate is controlled primarily by the k_3 (that corresponds to the segregated Y^{3+} ion effect) because the grain-growth behavior in 3YE shows the same tendency as that in 3 mol% Y-TZP. This discussion is consistent with that in Section 3.3. When the sintering temperature increases from 1300 to 1500 °C, the k_3 in 3YE increases almost the same tendency as that in 3 mol% Y-TZP and further the k_2 in 3YE also increases. This result reveals that when the sintering temperature increases, the grain-growth rate in 3YE becomes greater than that in 3 mol% Y-TZP because the contribution of the GBD term that corresponds to the segregated Al^{3+} ion effect increases with increasing sintering temperature.

The k_{03} in 3 mol% Y-TZP was also determined from the intercept of the straight line in Fig. 11 (Table 1). Both Q_3 and k_{03} of the LD term that corresponds to the segregated Y^{3+} ion effect in 3YE were greater than those in 3 mol% Y-TZP. The k_{03} is proportional to the product of the γ_{gb} and pre-exponential term in the diffusivity.[35,37] Therefore, the γ_{gb}s in 3YE and 3Y were examined by the thermal grooving technique. Fig. 12 shows the ϕ distributions on the thermally grooved grain boundary in 3YEs and 3Ys sintered at 1300 and 1500 °C for 2 h. Table 2 shows the average values of ϕ measured for 3Y and 3YE. At

Table 2
Average values of dihedral angles and normalized grain-boundary energies in 3YEs and 3Ys sintered at 1300 and 1500 °C for 2 h.

Specimen	Temperature (°C)	Average dihedral angle (°)		Normalized grain-boundary energy	
		ϕ	Standard deviation	γ_{ngb}	Standard deviation
3YE	1300	163.3	8.2	0.29	0.14
3YE	1500	159.9	8.1	0.35	0.14
3Y	1300	157.2	11.0	0.39	0.19
3Y	1500	156.6	10.9	0.40	0.18

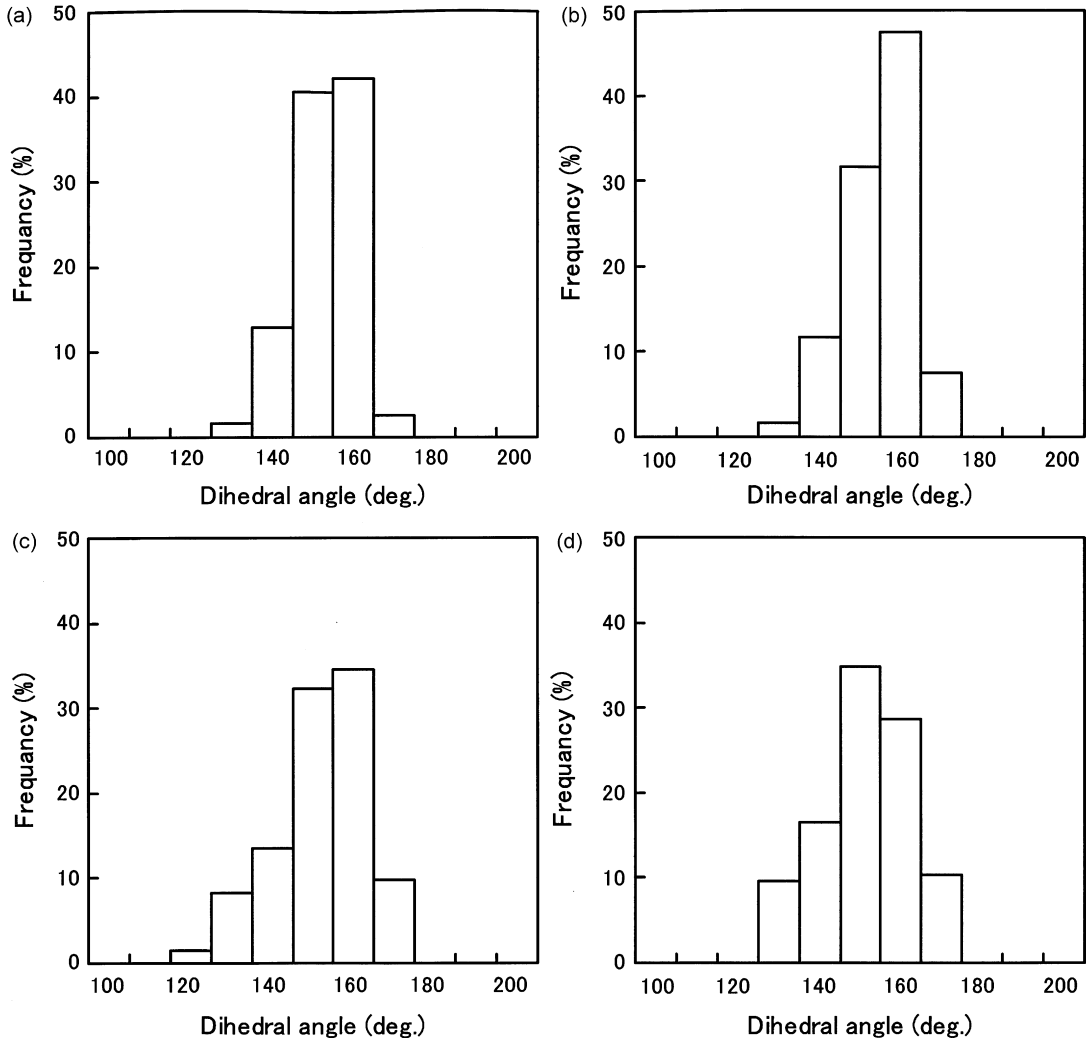

Fig. 12. Dihedral angle distributions on the thermally grooved grain boundary in 3YEs and 3Ys sintered at 1300°C and 1500 °C for 2 h: (a) 3YE-1300 °C, (b) 3YE-1500 °C, (c) 3Y-1300 °C, and (d) 3Y-1500 °C.

each sintering temperature, the ϕ in 3YE was grater than that in 3Y. Using the values determined of ϕ and Eq. (2), the average values of γ_{ngb} were estimated (Table 2). At each sintering temperature, the γ_{ngb} in 3YE was smaller than that in 3Y. The decrease in γ_{ngb} corresponds to that in γ_{gb},[20] which is caused by the grain-boundary segregation of Al^{3+} ions because Al^{3+} ions segregate along grain boundaries in 3YEs sintered at 1300 and 1500 °C for 2 h.[5,6] Therefore, the increase in k_{03} corresponds to that in the pre-exponential term in the diffusivity. According to a impurity-drag theory in Cahn,[38] the activation energy for the grain-boundary mobility is closely related to the segregation energy of the impurity on the grain boundary, which can be applicable to the grain-boundary segregation of Al^{3+} ions. Therefore, the increases in both Q_3 and k_{03} in 3YE is caused by Al^{3+} ions segregated along grain boundaries.

4. Conclusions

In the present study, the isothermal sintering behavior in 3 mol% Y-TZP doped with 0.3 mol% Al_2O_3 were investigated to verify the $T \rightarrow C$ phase-transformation behavior at the low sintering temperature of 1300 °C and clarify the grain-growth mechanism. The following conclusions were obtained.

(1) In the isothermal sintering condition of 1300 °C, the grain-growth rate was very limited. In the Y-TZP doped with Al_2O_3 sintered at 1300 °C for 50 h, Y^{3+} and Al^{3+} ions segregated along grain boundaries within the widths of about 10 and 6 nm, respectively. In grain interiors, the cubic-phase regions with high Y^{3+} ion concentrations were clearly formed adjacent to the grain boundary, which can be explained using the *GBSIPT* model. On the other hand, the modulated structure of the cubic phase was also clearly formed in grain interiors by spinodal decomposition. Therefore, in this isothermal sintering process, the cubic-phase regions in grain interiors not only are formed by the *GBSIPT* mechanism but also are formed by spinodal decomposition, which can be explained by the diffusion-acceleration effect of Al_2O_3-doping.

(2) The grain-growth behavior in Y-TZP doped with Al_2O_3 was analyzed using the rate equation that considered the solute-drag effect of segregated Y^{3+} ions (i.e., LD term) and the enhancing GBD effect of segregated Al^{3+} ions (i.e., GBD term). $Q_3 = 640$ kJ/mol and $\ln k_{03} = -11.1$ for LD term and $Q_2 = 588$ kJ/mol and $\ln k_{02} = -1.48$ for GBD term were determined. This result indicates that when the sintering temperature increases, the grain-growth rate in Al_2O_3-doped Y-TZP becomes greater than that in 3 mol% Y-TZP because the contribution of the GBD-acceleration effect of segregated Al^{3+} ions.

Acknowledgements

A part of this work was conducted in Center for Nano Lithography & Analysis, The University of Tokyo, and partly supported by the Grant-in-Aid for Scientific Research on Priority Areas "Nano Materials Science for Atomic-Scale Modification 474" from the Ministry of Education, Culture, Sports and Technology (MEXT) of Japan.

References

1. Tosoh Corporation, *Powders TZ series. Zirconia Catalog*, Tokyo, Japan; 2003.
2. Matsui K, Yamakawa T, Uehara M, Enomoto N, Hojo J. Mechanism of alumina-enhanced sintering of fine zirconia powder: influence of alumina concentration on the initial stage sintering. *J Am Ceram Soc* 2008;**91**:1888–97.
3. Sakka Y, Ishii T, Suzuki TS, Morita K, Hiraga K. Fabrication of high-strain rate superplastic yttria-doped zirconia polycrystals by adding manganese and aluminum oxides. *J Eur Ceram Soc* 2004;**24**:449–53.
4. Guo X, Waser R. Electrical properties of the grain boundaries of oxygen ion conductors: acceptor-doped zirconia and ceria. *Prog Mater Sci* 2006;**51**:151–210.
5. Matsui K, Horikoshi H, Ohmichi N, Ohgai M, Yoshida H, Ikuhara Y. Cubic-formation and grain-growth mechanisms in tetragonal zirconia polycrystal. *J Am Ceram Soc* 2003;**86**:1401–8.
6. Matsui K, Ohmichi N, Ogai M, Yoshida H, Ikuhara Y. Effect of alumina-doping on grain boundary segregation-induced phase transformation in yttria-stabilized tetragonal zirconia polycrystal. *J Mater Res* 2006;**21**:2278–89.
7. Tsubakino H, Nozato R. Effect of alumina addition on the tetragonal-to-monoclinic phase transformation in zirconia–3 mol% yttria. *J Am Ceram Soc* 1991;**74**:440–3.
8. Hodgson SNB, Cawley J, Clubley M. The role of Al_2O_3 impurities on the microstructure and properties of Y-TZP. *J Mater Process Technol* 1999;**92-93**:85–90.
9. Suzuki TS, Sakka Y, Morita K, Hiraga K. Enhanced superplasticity in a alumina-containing zirconia prepared by colloidal processing. *Scripta Mater* 2000;**43**:705–10.
10. Ross IM, Rainforth WM, McComb DW, Scott AJ, Brydson R. The role of trace additions of alumina to yttria-tetragonal zirconia polycrystals (Y-TZP). *Scripta Mater* 2001;**45**:653–60.
11. Guo X. Roles of alumina in zirconia for function applications. *J Am Ceram Soc* 2003;**86**:1867–73.
12. Matsui K, Yoshida H, Ikuhara Y. Isothermal sintering effects on phase transformation and grain growth in yttria-stabilized tetragonal zirconia polycrystal. *J Am Ceram Soc* 2009;**92**:467–75.
13. Matsui K, Ohmichi N, Ogai M, Yoshida H, Ikuhara Y. Grain boundary segregation-induced phase transformation in yttria-stabilized tetragonal zirconia polycrystal. *J Ceram Soc Jpn* 2006;**114**:230–7.
14. Matsui K, Yoshida H, Ikuhara Y. Grain-boundary structure and microstructure development mechanism in 2–8 mol% yttria-stabilized zirconia polycrystals. *Acta Mater* 2008;**56**:1315–25.
15. Yamaguchi T. Characterization techniques of ceramic: properties of sintered bodies. *Ceram Jpn* 1984;**19**:520–9.
16. Izumi F. Rietveld analysis programs RIETAN and PREMOS and special applications. In: Young RA, editor. *The Rietveld Method*. Oxford: Oxford University Press; 1993. p. 236–53.
17. Rietveld HM. A profile refinement method for nuclear and magnetic structures. *J Appl Crystallogr* 1969;**2**:65–71.
18. Hill JR. Data collection strategies: fitting the experiment to the need. In: Young RA, editor. *The Rietveld Method*. Oxford: Oxford University Press; 1993. p. 61–101.
19. Ohmichi N, Kamioka K, Ueda K, Matsui K, Ogai M. Phase transformation of zirconia ceramics by annealing in hot water. *J Ceram Soc Jpn* 1999;**107**:128–33.
20. Kuwabara A, Yokota S, Ikuhara Y, Sakuma T. Grain boundary energy and tensile ductility in superplastic cation-doped TZP. *Mater Trans* 2004;**45**:2144–9.
21. Yoshida H, Yokoyama K, Shibata N, Ikuhara Y, Sakuma T. High-temperature grain boundary sliding behavior and grain boundary energy in cubic zirconia bicrystals. *Acta Mater* 2004;**52**:2349–57.
22. Mullins WW. Theory of thermal grooving. *J Appl Phys* 1957;**28**:333–9.
23. Sakuma T, Yoshizawa Y, Suto H. The modulated structure formed by isothermal ageing in ZrO_2–5.2 mol% Y_2O_3 Alloy. *J Mater Sci* 1985;**20**:1085–92.
24. Sakuma T, Yoshizawa Y, Suto H. The metastable two-phase region in the zirconia-rich part of the ZrO_2–Y_2O_3 system. *J Mater Sci* 1986;**21**:1436–40.
25. Katamura J, Sakuma T. Thermodynamic analysis of the cubic–tetragonal phase equilibria in the system ZrO_2–$YO_{1.5}$. *J Am Ceram Soc* 1997;**80**:2685–8.
26. Shibata N, Katamura J, Kuwabara A, Ikuhara Y, Sakuma T. The intensity and resulting phase transition of cubic zirconia. *Mater Sci Eng A* 2001;**312**:90–8.
27. Levin EM, McMurdie HF. Al_2O_3–ZrO_2 (cont.) (Fig. Zr-084). In: Ondik HM, McMurdie HF, editors. *Phase diagrams for zirconium and zirconia systems*. OH: American Ceramic Society; 1998. p. 63.
28. Scott HG. Phase relationships in the zirconia–yttria system. *J Mater Sci* 1975;**10**:1527–35.
29. Ii S, Yoshida H, Matsui K, Ikuhara Y. Misfit dislocation formation at the c/t interphase boundary in Y-TZP. *J Am Ceram Soc* 2008;**91**:3810–2.
30. Sakka Y, Oishi Y, Ando K. Zr–Hf interdiffusion in polycrystalline, Y_2O_3–$(Zr + Hf)O_2$. *J Mater Sci* 1982;**17**:3101–5.
31. Sakka Y, Oishi Y, Ando K, Morita S. Cation interdiffusion and phase stability in polycrystalline tetragonal ceria–zirconia–hafnia solid solution. *J Am Ceram Soc* 1991;**74**:2610–4.
32. Yoshida H, Nagayama H, Sakuma T. Small dopant effect on static grain growth and flow stress in superplastic TZP. *Mater Trans* 2003;**44**:935–9.
33. Burggraff AJ, Winnubst AJA. Segregation in oxide surface, solid electrolytes and mixed conductors. In: Nowotny J, Dufour LC, editors. *Surface and near-surface chemistry of oxide materials*. Amsterdam: Elsevier Science Publishers B.V.; 1988. p. 449–75.
34. Shannon RD. Revised effective ionic radii and systematic studies of interatomic distances in halides and chalcogenides. *Acta Crystallogr* 1976;**A32**:751–67.
35. Brook RJ. The impurity-drag effect and grain growth kinetics. *Scripta Metall* 1968;**2**:375–8.
36. Nishizawa T. Grain growth in single- and dual-phase steels. *Tetsu-to-Hagane* 1984;**70**:194–202.
37. Brook RJ. Controlled grain growth. In: Wang FFY, editor. *Ceramic fabrication processes*. New York: Academic Press Inc.; 1976. p. 331–62.
38. Cahn JW. The impurity-drag effect in grain boundary motion. *Acta Metall* 1962;**10**:789–98.